# This is the author's peer reviewed, accepted manuscript. However, the online version of record will be different from this version once it has been copyedited and typeset.

PLEASE CITE THIS ARTICLE AS DOI: 10.1063/5.0167288

# High field suppression of bremsstrahlung emission in high-intensity laser-plasma interactions

M. Habibi, <sup>1</sup> A. Arefiev, <sup>2</sup> and T. Toncian <sup>1</sup>

<sup>1)</sup>Institute for Radiation Physics, Helmholtz-Zentrum Dresden-Rossendorf, Dresden 01328,

<sup>2)</sup>Department of Mechanical and Aerospace Engineering, University of California San Diego, La Jolla, CA 92093, IISA

(Dated: 18 September 2023

The interaction of high-intensity lasers with plasma is predicted to produce extreme quasi-static magnetic fields with magnitudes approaching Megatesla (MT) levels. In relativistically transparent plasmas, these fields can enhance direct laser acceleration and allow efficient gamma-ray emission by accelerated electrons. However, due to the so-called magnetic suppression effect, the magnetic field can also affect radiating electron trajectories and thus reduce the emission probability of the bremsstrahlung. This is the first study to examine the bremsstrahlung suppression mechanism in the context of high-intensity laser-plasma interactions. Our paper describes a new module that integrates the suppression effect into the standard bremsstrahlung module of the EPOCH particle-in-cell code by considering the impact of magnetic fields and extending the analysis to electric fields. We also investigate this suppressing mechanism's effect on the emitting electron's dynamics. Our findings show that this mechanism not only suppresses low-energy emissions but also has an impact on the dynamics of the radiating electrons.

### I. INTRODUCTION

Super-strong magnetic fields with a strength that is in the MT range and above are typically associated with astrophysical environments, where they play a key role in a variety of phenomena<sup>1-6</sup>. Until recently, this field strength was inaccessible to laboratory experiments. However, recent developments in high-power laser technology<sup>7-12</sup> have enabled multiple concepts that can be employed to generate slowly evolving (compared to the laser period) magnetic fields with a strength reaching the MT-level<sup>13-17</sup>.

One such concept considered in this paper relies on the phenomenon of relativistically induced transparency<sup>18–25</sup> to facilitate the volumetric interaction of a high-intensity laser pulse with a dense plasma. The high-intensity laser electric field energizes plasma electrons, making them relativistic and thus changing the optical properties of the plasma. As a result, a classically opaque plasma can become transparent, allowing the laser pulse to propagate and drive a longitudinal electron current. Due to the high electron density, this current can be sufficiently strong to generate an MT-level azimuthal magnetic field. The combination of the oscillating laser fields and the quasi-static plasma magnetic field creates favorable conditions for enhanced energy gain by plasma electrons. It has been shown using particle-in-cell (PIC) simulations that the already accessible laser intensities are sufficient to produce a large population of energetic electrons whose energies are hundreds of MeV.

The energetic electrons have the potential to emit energetic gamma rays when deflected by magnetic or electric fields, which opens a path for creating an efficient laser-driven gamma-ray source. It has been shown using PIC simulations that electron deflections by the macroscopic strong plasma magnetic field lead to synchrotron emission of multi-MeV photons <sup>17,26–28</sup>. The photon population can be so energetic and dense that photon-photon collisions yield an appreciable number of electron-positron pairs <sup>29–32</sup>. The electrons can also

be deflected by plasma ions, leading to the bremsstrahlung emission of gamma rays, where the deflection is caused by the microscopic electric field of an ion. The typical implementation of the bremsstrahlung in PIC codes used for laser-plasma simulations ignores any suppression due to the presence of extreme macroscopic fields. The purpose of this paper is to examine whether this is justified and, if not, to provide an assessment of possible suppression.

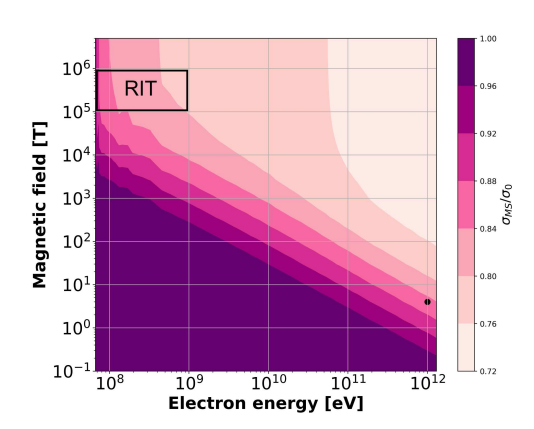


FIG. 1. Magnetic suppression of bremsstrahlung emission. Color-coded is the relative reduction of the bremsstrahlung cross-section as a function of the electron energy and macroscopic magnetic field experienced by the electron, where  $\sigma_{MS}$  is the cross-section in the presence of the magnetic field (MS stands for the magnetic suppression effect) and  $\sigma_0$  is the cross-section in the absence of the field. Highlighted are 1) the parameters at the Compact Muon Solenoid experiment at the Large Hadron Collider (marked as LHC) and 2) the parameters expected for high-intensity laser-plasma interactions due to the relativistically induced transparency (marked as RIT).

Physics of Plasmas

This is the author's peer reviewed, accepted manuscript. However, the online version of record will be different from this version once it has been copyedited and typeset

The concept of bremsstrahlung suppression is well-known in the field of high-energy physics. The photon emission during bremsstrahlung takes place over an extended distance called the formation length  $l_{f0}$ . If the electron trajectory is disrupted during the time that the electron travels the formation length, then the emission becomes suppressed as a result of the disruption. The disruption can arise from relatively frequent collisions with atoms or ions in a dense medium, as in the case of the Landau-Pomeranchuk-Migdal effect. A macroscopic magnetic field can be another source of disruption. The resulting magnetic suppression of bremsstrahlung has been extensively examined in Ref. [33].

Figure 1 shows how the total bremsstrahlung cross-section changes for a given electron energy in the presence of a static uniform magnetic field due to suppression. The plotted ratio is the relative reduction in the total emission due to magnetic suppression. It is instructive to examine high-energy physics scenarios where suppression becomes important. The suppression is significant for high-energy cosmic rays  $(10^{20} \text{ eV})$ in the earth's magnetic field  $(50 \mu T)^{34}$ . In contrast to that, the bremsstrahlung emission by the electrons generated by the Large Hadron Collider (LHC) is unaffected by the earth's magnetic field. However, the 4 T magnetic field at the Compact Muon Solenoid experiment at the LHC is sufficient to suppress the emission of 1 TeV electrons.

The general trend for magnetic suppression is that the strength of the magnetic field able to induce the effect goes up as the electron energy goes down. This is one of the reasons why the magnetic suppression effect has been so far ignored for the energetic electrons generated in laser-plasma interactions. Even for 10 GeV electrons, which is currently the upper limit of what can be achieved experimentally, the magnetic field strength has to be in the range of 103 T for the suppression to be noticeable. Such a field is inaccessible to conventional magnets. However, the plasma magnetic fields in the regime of relativistically induced transparency can be much stronger than 10<sup>3</sup> T, as discussed earlier, which suggests that the effect of magnetic suppression can come into play. Indeed, as shown in Fig. 1, the bremsstrahlung cross-section for 300 MeV electrons-the energy not uncommon for highintensity laser-plasma interactions-should be suppressed by 20% in a 200 kT plasma magnetic field.

The goal of this paper is to quantitatively examine the suppression of bremsstrahlung in high-intensity laser-plasma interactions involving MT-level magnetic fields. Such interactions necessarily involve electric and magnetic fields, so we have generalized the analysis employed for the magnetic suppression to also include a strong electric field. To selfconsistently evaluate the suppression, we have upgraded the standard bremsstrahlung module of the EPOCH particle-incell code<sup>35,36</sup> to include the suppression effect by a combination of electric and magnetic fields. Two-dimensional PIC simulations performed with this module have revealed that the bremsstrahlung emission inside the laser-irradiated plasma can become noticeably suppressed, with the total emitted energy decreasing by as much as 30% for some electrons. The reduction primarily impacts the sub-MeV part of the emitted photon spectrum. Even though the synchrotron emission dominates over the bremsstrahlung in the considered regime, our results provide new insights into the bremsstrahlung emission in high-intensity laser-plasma interactions. Specifically, our results indicate that the conventional implementation of bremsstrahlung used by PIC codes needs to be adjusted to include the discussed suppression effect.

2

The rest of the paper is organized as follows. In Section II, we provide a qualitative description of the electric-magnetic suppression mechanism for high-energy electron emissions, and in Section III, we discuss the routine of implementing these mechanisms in the EPOCH code. This discussion sets the context for the analysis that follows. Section IV presents simulation results of high-intensity laser pulse interactions with a structured plasma target obtained by using the modified bremsstrahlung module. Finally, a summary and conclusions are given in Section V.

### II. MODEL FOR BREMSSTRAHLUNG SUPPRESSION BY MACROSCOPIC ELECTRIC AND MAGNETIC FIELDS

In this section, we present a derivation of the suppression factor due to the presence of external fields, following an approach similar to that of Ref. [33]. We start by discussing formation length and then derive a general form of suppression factor. We apply it to the regime where macroscopic electric and magnetic fields are both present. In the absence of an electric field, we show that our derivations converge to the previously described magnetic suppression effect<sup>33</sup>

The term bremsstrahlung refers to the radiation emitted by an electron as a result of its interaction with the microscopic electric field of an ion. The emission takes place over an extended time interval that sets the so-called formation length, or, more generally, the coherence length  $l_{f_0}$  that the electron must travel during the emission process. The formation length appears in classical and quantum-mechanical calculations. We use a quantum-mechanical approach here to find the formation length.

We begin by considering the conservation of energy in an isolated electron-ion collision, where an ultra-relativistic electron with energy  $\varepsilon_e$  collides with an initially immobile ion and emits a forward-directed low-energy photon with energy  $\varepsilon_{\gamma}$ :

$$\varepsilon_e = \varepsilon_e' + \varepsilon_\gamma,$$
 (1)

where  $\varepsilon'_{e}$  is the energy of the scattering electron. Note that the ion recoil energy in the elastic scattering situation can be estimated as  $O(10^{-4} \times \varepsilon_e/\gamma^2)$ , where  $\gamma$  is the relativistic factor, for relativistic electron scattering at a small angle  $\sim O(1/\gamma)$ from a Carbon ion. This is even smaller for inelastic scattering, so it is neglected in Eq. (1). Furthermore, the conservation of momentum is written as,

$$\mathbf{p}_e = \mathbf{p}_e' + \mathbf{p}_\gamma + \mathbf{p}_i', \tag{2}$$

Here,  $\mathbf{p}_{e}$  is the momentum of the electron prior to the collision, and  $\mathbf{p}_e'$ ,  $\mathbf{p}_{\gamma}$ , and  $\mathbf{p}_i'$  are the momenta of the electron, emitted photon, and ion after the collision.

For the sake of simplicity, it is assumed that this process occurs in the (x,y) plane, with the incoming electron propagating along the x-axis. The x and y components of Eq. (2)

$$p_{e,x} - p'_{i,x} = p'_e \cos \theta + p_{\gamma} \cos \vartheta, \tag{3}$$

$$p'_{i,y} = p'_e \sin \theta + p_\gamma \sin \vartheta, \tag{4}$$

where  $\theta$  is the scattering angle for the electron and  $\vartheta$  is the angle of photon emission. By squaring both sides of these equations and then adding the resultant equations, we obtain the following relation:

$$p_{e,x}^2 + p_i'^2 - 2p_{e,x}p_{i,x}' = p_e'^2 + p_\gamma^2 + 2p_e'p_\gamma\cos\Theta,$$
 (2)

where  $\Theta \equiv \theta - \vartheta$ . By employing Eq. (1) and considering  $p^2 = \frac{\varepsilon^2}{c^2} - m_e^2 c^2$ , and neglecting  $p_i^2$  due to its negligible magnitude in comparison, we derive the following relation for ultrarelativistic electron ( $\varepsilon_e, \varepsilon'_e \gg m_e c^2$ ):

$$\frac{p'_{l,x}}{m_e c} \approx \frac{1}{2} \frac{\varepsilon_{\gamma} m_e c^2}{\varepsilon_e (\varepsilon_e - \varepsilon_{\gamma})} + \left(1 - \frac{\varepsilon_{\gamma}}{\varepsilon_e}\right) \frac{\varepsilon_{\gamma}}{m_e c^2} [1 - \cos\Theta], \quad (6)$$

where  $m_e$  is the electron mass and c is the speed of light. The maximal probability of emission of a bremsstrahlung photon is associated with the maximal coherence length and the related minimal momentum transfer to the ion. The minimal value of  $p'_{i,x}$  is obtained when both  $\theta$  and  $\vartheta$  are zero. In this case, Eq. (6) reduces to

$$\frac{p'_{i,\min}}{m_e c} = \frac{1}{2} \frac{\varepsilon_{\gamma} m_e c^2}{\varepsilon_e (\varepsilon_e - \varepsilon_{\gamma})},\tag{7}$$

Using the uncertainty principle, we find that the maximum coherence length is

$$l_{f_0} \approx \frac{\hbar}{p'_{i,\min}} = \frac{2\hbar}{m_e c} \frac{\varepsilon_e(\varepsilon_e - \varepsilon_{\gamma})}{\varepsilon_{\gamma} m_e c^2}, \tag{8}$$

where  $\hbar$  is the Planck constant. Note that  $\hbar/m_e c \approx 3.86 \times$ 10<sup>-13</sup> m is the Compton wavelength of the electron. For  $\varepsilon_e = 100$  MeV and  $\varepsilon_{\gamma} = 0.1$  MeV, we have  $l_{f_0} \approx 0.15$  µm, so the formation length is a non-negligible fraction of the wavelength ( $\sim 1 \mu m$ ) for an optical laser. In contrast, because the transverse momentum transfer is substantially greater than its longitudinal counterpart, the associated transverse formation length  $\hbar/p'_{i,v}$  becomes considerably shorter. Therefore, it is considered to be of less significance in this context

If macroscopic fields, such as electric and magnetic fields, exert additional influence on the electron during its interaction with the ion, the derived formation length can be reduced. In this circumstance, the scattering of the electron is affected not only by the Coulomb force of the ion, but also by the macroscopic fields. We derive an expression for the suppressed formation length by substituting  $p'_{i,x}$  from Eq. (6) into the uncertainty principle relation and employing  $l_{f_0}$  as defined in Eq. (8). The resulting expression for the suppressed formation length  $l_f$  is

$$l_f \approx \frac{\hbar}{p'_{i,x}} = \frac{l_{f_0}}{1 + \alpha_1 [1 - \cos\Theta]},\tag{9}$$

where  $\alpha_1 = 2(\varepsilon_e - \varepsilon_{\gamma})^2/m_e^2 c^4$ . This equation can be applied to define the suppression factor as the ratio of formation length in a disturbed state to formation length in an undisturbed state (see Ref. [33] for a supporting discussion):

$$S = l_f / l_{f_0} = [1 + \alpha_1 [1 - \cos \Theta]]^{-1}, \qquad (10$$

To examine the impact of external macroscopic fields, we relate  $\Theta$  to a deflection angle accumulated during the emission process. We set  $\Theta = \arctan(|\Delta p_{\perp}/p|)$ , where  $\Delta p_{\perp}$  is the transverse change in momentum due to the interaction with the macroscopic fields. We estimate it as

$$\Delta p_{\perp} \approx |e|\tilde{\mathcal{E}}_{\rm ext}\Delta t,$$
 (11)

3

where

$$\tilde{\mathcal{E}}_{\text{ext}} \equiv |(\mathbf{E} + \mathbf{v} \times \mathbf{B})_{\perp}| \tag{12}$$

and

$$\Delta t \approx l_f/2c$$
 (13)

is the travel time over half the formation length. After taking into account that the electron is ultra-relativistic, we find that

$$\Theta = \arctan\left(|e|\tilde{\mathcal{E}}_{\text{ext}}l_f/2\gamma m_e c^2\right) \tag{14}$$

We substitute this expression into Eq. (10) to obtain

$$S_{\tilde{\mathcal{E}}}\left(\varepsilon_{e}, \varepsilon_{\gamma}, \tilde{\mathcal{E}}_{\text{ext}}\right) = \left[1 + \alpha_{1} \left(1 - \frac{1}{\sqrt{1 + (\alpha_{2}l_{f})^{2}}}\right)\right]^{-1}$$

$$= \left[1 + \alpha_{1} \left(1 - \frac{1}{\sqrt{1 + (\alpha_{2}l_{f_{0}}S_{\tilde{\mathcal{E}}})^{2}}}\right)\right]^{-1},$$
(15)

where  $\alpha_2 = \tilde{\mathcal{E}}_{\rm ext} m_e c / 2 \gamma E_{\rm cr} \hbar$  and  $E_{\rm cr} = m_e^2 c^3 / e \hbar = 1.3 \times$ 10<sup>18</sup> V/m denotes the Schwinger critical electric field. In Eq. (15), we have obtained a concise form for the electricmagnetic suppression factor,  $S_{\tilde{e}}$ , by using the trigonometric equation,  $\cos(\arctan(x)) = 1/\sqrt{1+x^2}$ , which relates the tangent and cosine functions. Equation (15) can be applied as a multiplicative correction factor to the original differential cross-section,

$$\frac{d\sigma_{\tilde{\mathcal{E}}}}{d\varepsilon_{\gamma}} = S_{\tilde{\mathcal{E}}} \left( \varepsilon_{e}, \varepsilon_{\gamma}, \tilde{\mathcal{E}}_{\text{ext}} \right) \frac{d\sigma_{0}}{d\varepsilon_{\gamma}}, \tag{16}$$

with  $\sigma$  and  $\sigma_0$  being the total cross-sections with and without suppression effect. It is important to stress that significant suppression already occurs at small deflection angles. It follows from Eq. (6) that for  $\Theta \ll 1$  we have

$$\frac{p_{i,x}'}{m_e c} = \frac{1}{2} \frac{\varepsilon_{\gamma} m_e c^2}{\varepsilon_e (\varepsilon_e - \varepsilon_{\gamma})} + \frac{1}{2} \frac{\varepsilon_e - \varepsilon_{\gamma}}{\varepsilon_e} \frac{\varepsilon_{\gamma}}{m_e c^2} \Theta^2.$$
 (17)

The deflection significantly alters the momentum exchange and thus disrupts the emissions when the second term on the

$$\Theta \gtrsim m_e c^2 / \varepsilon_e$$
. (18)

The quantity on the right-hand side is very small for an ultrarelativistic electron, which confirms that appreciable suppression occurs at small Θ.

To conclude this section, we consider a better-known regime where the macroscopic field is a static external magnetic field,  $B_{\text{ext}}$  so that  $\Theta = \arctan(|e|B_{\text{ext}}l_f/2\gamma m_e c)$ . For a small deflection angle, we have  $\Theta \approx |e|B_{\rm ext}l_f/2\gamma m_e c$ . We now assume that the suppression is significant, which means that  $p'_{i,x}$  given by Eq. (17) is determined by the  $\Theta^2$ -term. We use this value to find  $l_f$  and then to calculate the suppression fac-

$$S_B\left(\varepsilon_e, \varepsilon_\gamma, B_{\rm ext}\right) \approx \left[\frac{\varepsilon_\gamma m_e c^2}{\varepsilon_e^2} \frac{B_{\rm cr}}{B_{\rm ext}}\right]^{2/3},$$
 (19)

where  $B_{\rm cr} = m_e^2 c^2 / e\hbar = 4.4 \times 10^9$  T is the Schwinger critical magnetic field. Here we explicitly took into account that  $\varepsilon_e\gg arepsilon_\gamma$  to simplify the expression. This expression for the suppression factor matches the one given in Ref. [33] in the limit of  $\varepsilon_e \gg \varepsilon_{\gamma}$ . In the following Section, we will explain how both of the aforementioned suppression effects were implemented in a PIC simulation code.

### III. BREMSSTRAHLUNG SUPPRESSION IMPLEMENTATION IN A PIC CODE

For a quantitative analysis of the relevance of suppression of bremsstrahlung in the regime of relativistic laser-plasma interactions, we have chosen to study this effect with the aid of PIC simulations. In particular, we have modified the bremsstrahlung module of the EPOCH (the Extendable PIC Open Collaboration) code. 35,36 In the standard module of bremsstrahlung of EPOCH, two Monte-Carlo simulation steps are used to calculate the emission of a photon. The first step evaluates the emission probability, and if a photon is generated, the second step will sample the resulting spectral distribution.

For computational reasons, the total bremsstrahlung crosssections and the corresponding cumulative distribution of the differential cross-section as a function of the photon energy  $CDF(\varepsilon_e, \varepsilon_{\gamma})$  are tabulated in EPOCH following the Seltzer and Berger data set37 and loaded at the initialization stage of the code. As an additional variable, we have also embedded the suppression factors Eq. (15), computed using the iterative Newton-Raphson numerical method outside of EPOCH, for the electric and magnetic suppression effect and also its corresponding values for the magnetic suppression effect. In this case, the dimension of the EPOCH tabulated data is increased to account for the suppression factors. The total cross-sections and the corresponding cumulative distribution of the differential cross-sections are then modified to reflect the suppression models employed.

### Magnetic Suppression (MS) effect implementation

To include the effect of magnetic suppression, we first obtain the bremsstrahlung differential cross-sections by multiplying total cross-sections by the differential of cumulative distribution functions with respect to photon energies. Then, we correct the differential cross-sections by multiplication with the precalculated suppression factors, resulting in the modified differential cross-sections  $d\sigma_{\rm MS}/d\varepsilon_{\gamma}$ . 'MS' represents the magnetic suppression effect.

In the next step, the adjusted differential cross-sections are integrated over photon energy to produce total cross-sections  $\sigma_{\rm MS}(\varepsilon_e,B_{\rm ext})$ , with the additional dependence on the magnetic field. The new modified tables are returned to the code, replacing the original tables and concluding the bremsstrahlung routine setup step. Further, we had to modify the routines interpolating the discrete tabulated data, used at the time of code execution, to account for the higher dimension due to the addition of the field dependence.

### Electric and Magnetic Suppression (EMS) effect implementation

The implementation of the electric and magnetic suppression model into the EPOCH code, however, adds considerable complexity to the methodology of the previous Section III A. As a first step, the original total cross-section and corresponding cumulative distribution tables are revised using precalculated suppression factors from Eq. (15) to account for the new dependencies,  $\sigma_{\rm EMS}(\varepsilon_e, \tilde{\varepsilon}_{\rm ext})$  ('EMS' represents the electric and magnetic suppression effect) and CDF( $\varepsilon_e, \varepsilon_{\gamma}, \tilde{\varepsilon}_{\text{ext}}$ ).

As the EPOCH standard bremsstrahlung module has been implemented inside the PIC loop, we directly evaluate the electron deflection angle from the transverse part (compared to the electron velocity vector) of the Lorentz force from the change of momentum,  $\Theta_{
m pic} = \Delta p_{\perp}/p$ , calculated by the particle pusher of EPOCH for each simulation time-step ( $\Delta t$ ). For photons with energies of  $\varepsilon_{\gamma} = 10 \text{ KeV}$  and  $\varepsilon_{\gamma} = 100 \text{ KeV}$  emitted by an electron with  $\dot{\varepsilon}_e = 100$  MeV, the formation time is typically 5 fs and 0.5 fs, respectively. This time is reduced to 0.049 fs and 0.0045 fs for photons with  $\varepsilon_{\gamma} = 1 \text{ MeV}$ and  $\varepsilon_{\gamma} = 10$  MeV, respectively, for the same radiating electron. These times must be considered in relation to the typical temporal resolution of PIC, which is, for the used simulation setup,  $\Delta t = 0.018$  fs. Therefore, the deflection angle  $\Theta_{pic}$  must be scaled now by the formation time of the bremsstrahlung  $t_{f_0}$ to the deflection angle  $\Theta_{EMS}$  used as input for the corresponding tables. This step adds complexity to the Monte-Carlo algorithm once again. The formation time,  $t_{f_0}$ , is dependent on the emitted photon energy. As previously stated, the emitted photon energy is sampled in the last step of the EPOCH bremsstrahlung Monte-Carlo algorithm and is not available at this time. As a solution to circumvent this problem, we implemented an additional Monte-Carlo step to evaluate a statistically relevant photon spectral energy distribution. In order not to over-bias the significance of low energy photons, we first construct the marginal density function  $\mathscr{P}(\varepsilon_e, \varepsilon_\gamma)$  by integrat-



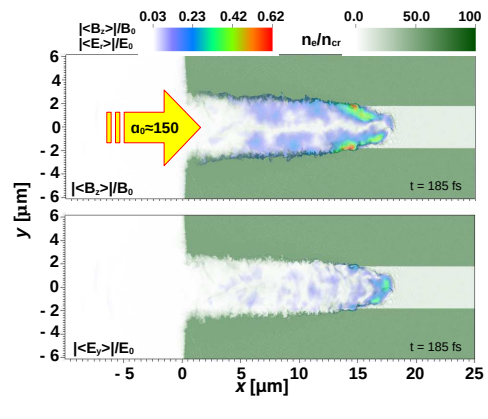


FIG. 2. A snapshot of the simulation setup at 185 fs where a high-intensity laser pulse  $I_L = 5 \times 10^{22}$  W/cm²  $(a_0 \approx 150)$  is propagating through an initially uniform relativistically transparent narrow channel  $(n_e = 20n_{\rm cr})$  surrounded by a relativistically over-critical bulk  $(n_e = 100n_{\rm cr})$  while generating a strong azimuthal magnetic field (upper panel), and a radial electric field (lower panel) shown as an averaged over one laser period.

ing  $\tilde{\mathcal{E}}_{ext}$  out of  $\frac{d\sigma_{EMS}}{d\epsilon_{\gamma}}(\varepsilon_{e}, \varepsilon_{\gamma}, \tilde{\mathcal{E}}_{ext})$ . Following that, we calculate the marginal cumulative distribution function CDF<sub>marg.</sub>( $\varepsilon_{e}, \varepsilon_{\gamma}$ ) for sampling photon energy, as required for determining  $\tilde{\mathcal{E}}_{ext}$  from the scaled deflection angle  $\Theta_{EMS}$ .

Upon finding  $\tilde{\mathcal{E}}_{\text{ext}}$ , the next steps of the implementation are identical to those of the preceding Section III A, except for replacing  $B_{\text{ext}}$  with  $\tilde{\mathcal{E}}_{\text{ext}}$  in the method description.

### IV. RESULTS AND DISCUSSION

In order to validate our implementation and examine the impact of the bremsstrahlung suppression on laser-plasma interactions, we have performed a set of 2D-PIC simulations with and without suppression effects. To keep things simple, we will refer to simulations without suppression as EPOCH, simulations with electric-magnetic suppression as EMS, and simulations with only magnetic suppression as MS. We have chosen the regime of relativistically induced transparency with a configuration similar to that used in Refs. [26] and [28]. In this setup, a Petawatt-class laser pulse with a peak intensity of  $5 \times 10^{22}$  W/cm<sup>2</sup>, a wavelength of 800 nm, a normalized laser amplitude of  $a_0 \approx 150$ , and a pulse duration of 30 fs irradiates a channel with an electron density of  $n_e = 20n_{cr}$  in a structured target shown in Fig. 2. Here,  $n_{\rm cr} \approx 1.74 \times 10^{21}$ cm<sup>-3</sup> is the classical critical density. The target is initialized as a fully ionized Carbon plasma (Z = 6). Note that the plasma is relativistically transparent to a laser pulse with frequency  $\omega_L$  if the electron density,  $n_e$ , satisfies the condition  $n_e \ll \gamma_{av} n_{cr}$ , where  $\gamma_{av}$  is the characteristic (average) relativistic factor of the electron population and  $n_{\rm cr} = m_e \omega_L^2 / 4\pi e^2$  is the classical critical density. In the case of a laser-irradiated plasma, the electrons are heated by the electric field of the laser, so we roughly expect  $\gamma_{\rm av} \sim a_0$ , where  $a_0$  is the normalized laser amplitude. Then the relativistic transparency condition reads  $n_e \ll a_0 n_{\rm cr}$ .

Such a regime of interaction has been shown to sustain quasi-static MT-level magnetic fields and generate ultrarelativistic electrons via the direct laser acceleration assisted by the magnetic field<sup>17</sup>. The color in Fig. 2(a) represents the amplitude of the quasi-static azimuthal magnetic field  $|\langle B_z \rangle|$  in the (x,y) plane at z=0 generated by the longitudinal electron current within the channel. The field is normalized to  $B_0$ . Additionally, the laser beam produces a transverse quasi-static electric field  $|\langle E_y \rangle|$ , whose profile is depicted in Fig. 2(b). The detailed parameters of the two-dimensional simulations are given in Table I.

TABLE I. Parameters of 2D-PIC simulations.

Parameters	Values
General parameters:	
Computational cells $(n_x \times n_y)$	2250 800
Length of simulation domain	$x \in (-15, 30)  \mu \text{m}$
Width of simulation domain	$y \in (-8, 8) \ \mu m$
Laser parameters:	
Peak intensity	$I_0 = 5 \times 10^{22} \text{ W/cm}^2$
Wavelength	$\lambda_{\mathrm{L}} = 800 \; \mathrm{nm}$
Pulse duration	30 fs
Focal spot size	2.2 μm
Location of the focal plane	$x = 0 \mu m$
Target parameters:	
Target length (x)	30 μm
Target width (y)	16 μm
Channel radius	$R_{\rm ch} = 1.8~\mu \rm m$
Composition	$C^{6+}$ and electrons
Channel density	$n_e = 20n_{\rm cr}^{\ a}$
Bulk density	$n_e = 100n_{\rm cr}$

<sup>&</sup>lt;sup>a</sup> For the considered vacuum laser wavelength,  $\lambda_{\rm L}$  the critical density is  $n_{\rm cr}\approx 1.74\times 10^{21}~{\rm cm}^{-3}$ 

It is important to highlight that the dominant radiation mechanism in the considered regime is synchrotron radiation<sup>26</sup>. Wan et al.<sup>38</sup> demonstrated that this emission becomes the dominant process at laser intensities  $I_L \ge 10^{21} \text{ W/cm}^2$  (for 1  $\mu$ m-thick Al) and  $I_L \ge 10^{22}$  W/cm<sup>2</sup> (for 1  $\mu$ m-thick Au) targets. However, recent research conducted by Martinez et al.<sup>39</sup> has found a regime where the roles of bremsstrahlung and synchrotron emission are reversed, leading to bremsstrahlungdominated radiation mechanisms. Using simulations with a fixed set of laser parameters ( $I_L = 10^{22} \text{ W/cm}^2$ ) and a soliddensity copper plasma slab with a thickness of 16 nm <  $l \leq 5$  µm, they investigated the impact of target thickness on laser-plasma interactions. By comparing synchrotron and bremsstrahlung emission, they discovered that the efficiency of bremsstrahlung gradually increases with thicker targets and begins to predominate synchrotron radiation at approximately  $(l \approx 1 - 2 \mu m)$ . Even though the target used in this study does not provide a sufficiently strong magnetic field for investigating the magnetic suppression effect, this significant find-

ing demonstrates the importance of studying bremsstrahlung emission in situations where synchrotron radiation has been assumed to be the predominant form of radiation.

### Macroscopic impact of the suppression effects

To illustrate the bremsstrahlung suppression effect on a macroscopic level, we examined the photon emission within the channel of the target where a strong azimuthal magnetic field is generated. The recoil energy, i.e., the energy lost when an electron emits photons, was ignored for both simulations with and without the bremsstrahlung suppression effect in order to preserve the electron distributions as similar as possible between these simulation runs. Since the emission probability of a radiating electron is determined over the history of the so-called optical depth<sup>36</sup>, the emission characteristics are not only determined by the instantaneous environment of the emitting electron but by the whole history between the emissions. Therefore, between each emission time in the bremsstrahlung module of EPOCH, we calculate the average electron energy  $\langle \varepsilon_e \rangle$ , and the average of the electric  $\langle \tilde{\varepsilon} \rangle$  and magnetic  $\langle B_z \rangle$  field strengths experienced by radiating parent electrons prior to emission. Then, we save them as new particle properties alongside other photon characteristics so that we can use them to analyze the emitted photons.

We start our analysis of the photon emission by considering a subset of electrons with average energies,  $\langle \varepsilon_e \rangle$ , between 95 MeV and 105 MeV, over emission times. We further limit the subset by only considering those electrons that have sampled before photon emission and have averaged normalized fields with values of 0.29 - 0.31 for  $|\langle \tilde{\mathcal{E}} \rangle|/E_0$  for the electric and magnetic model and  $|\langle B_z \rangle|/B_0$  for the magnetic suppression model.  $E_0$  and  $B_0$  denote the maximal amplitude of the laser field for the used laser intensity  $I_0$ , in our case  $E_0 \approx 6.13 \times 10^{14}$  V/m and  $B_0 \approx 2.04$  MT. As we restrict our analysis to the same effective field strength and electron properties, we anticipate almost similar results for both models.

Figures 3(a) and (d) show the simulated energy distribution of bremsstrahlung for the MS and EMS models, respectively. There is a clear deviation in the number of low-energy photons with energies below 2.7 MeV for both models when the suppression effects are included, compared to the reference runs (EPOCH). The deviation increases as the photon energies decrease. Figures 3(b) and (e) show the total number of photons with  $\varepsilon_{\gamma}^* < \varepsilon_{\gamma}$  as a function of  $\varepsilon_{\gamma}$ , where

$$N_{\gamma}(\varepsilon_{\gamma}^* \le \varepsilon_{\gamma}) \equiv \int_{\varepsilon_{\gamma_{cut}}}^{\varepsilon_{\gamma}} \left(\frac{dN_{\gamma}}{d\varepsilon_{\gamma}^*}\right) d\varepsilon_{\gamma}^*.$$
 (20)

where  $\varepsilon_{\text{Yeut}}$  is the minimum energy of the emitted photon. While the EMS and the MS simulations lead predominately to a reduction in photon yield for the low-energy photons, the overall spectral shapes of bremsstrahlung are inverse exponential, resulting in a significant reduction of the total number of photons radiated. For the subsets shown, the reduction is  $\triangle N_{\gamma} = 36.25\%$  for the MS and  $\triangle N_{\gamma} = 50.44\%$  for the EMS models. The magnitude of the suppression in simulations was also measured by the ratio of the spectral density of the generated photons with and without the suppression effects [see the filled blue circles in Fig. 3(c) and (f)]. These series of data points obtained from the simulations were fitted with the analytical function of the suppression factor, given by Eq. (15). To do so, the photon energy is treated as the independent variable, and the optimal parameters for the average electron energy, magnetic, and electric fields are determined. These fitted parameters recover the subset that we had previously employed to constrain the photon analysis. In the next step, we have removed the subset restriction from the average field strength and have analyzed again the photons generated by electrons with an average energy  $\langle \varepsilon_e \rangle$  between 95 MeV and 105 MeV. We observed still significant suppression of  $\triangle N_{\gamma} = 37.10\%$  for the MS and  $\triangle N_{\gamma} = 35.65\%$  for the EMS models.

To rule out artificially biasing the significance as a result of the prior restrictions of our analysis, we conducted additional simulations to quantify the robustness of the suppression effects in the relativistically induced transparency regime, including the recoil of photon emission onto the parent electron. Further, we analyzed all emissions inside the  $20n_{cr}$  initial density channel independently of the emitting electron energies. Overall, we found that the low-energy emissions are still significantly suppressed, and a comparison of their accumulated number of photons reveals that  $\triangle N_{\gamma} = 17.43\%$  and  $\triangle N_{\gamma} =$ 19.11% fewer photons are emitted when the MS or EMS effect is considered, respectively, compared to  $\triangle N_{\gamma} = 18.35\%$ and  $\triangle N_{\gamma} = 20.77\%$  when the recoil is ignored. In addition, we examined the suppression effects of bremsstrahlung for a target without a channel, a bulk foam with an initial electron density of  $n_e = 20n_{cr}$ . We analyzed all electrons and emissions for the entire simulation box in this case. As a result, we observed a global reduction in the total number of photons of  $\triangle N_{\gamma} = 15.27\%$  for the EMS and  $\triangle N_{\gamma} = 14.14\%$  for the MS models. In summary, we have successfully benchmarked our implementation against the theory and have also demonstrated a substantial suppression of bremsstrahlung in various simulations in the relativistically induced transparency regime.

### Microscopic impact of the suppression effects

In the previous Section IV A, we showed that, on a macroscopic level, the yield of bremsstrahlung is affected by the consideration of the bremsstrahlung suppression effects. The current section will investigate in more detail the role of magnetic and electric fields in the bremsstrahlung suppression for the given setup. It will also answer whether the reduction of bremsstrahlung-associated energy losses is beneficial for electron acceleration or not. We begin our examination by investigating the microscopic dynamics of emitting electrons. As the suppression levels for both magnetic suppression and electric and magnetic suppression are very similar, we first follow the spatial and temporal history of selected electrons and analyze the role of each field component for the electron acceleration and thus its impact on the bremsstrahlung suppression.

# This is the author's peer reviewed, accepted manuscript. However, the online version of record will be different from this version once it has been copyedited and typeset.

PLEASE CITE THIS ARTICLE AS DOI: 10.1063/5.0167288

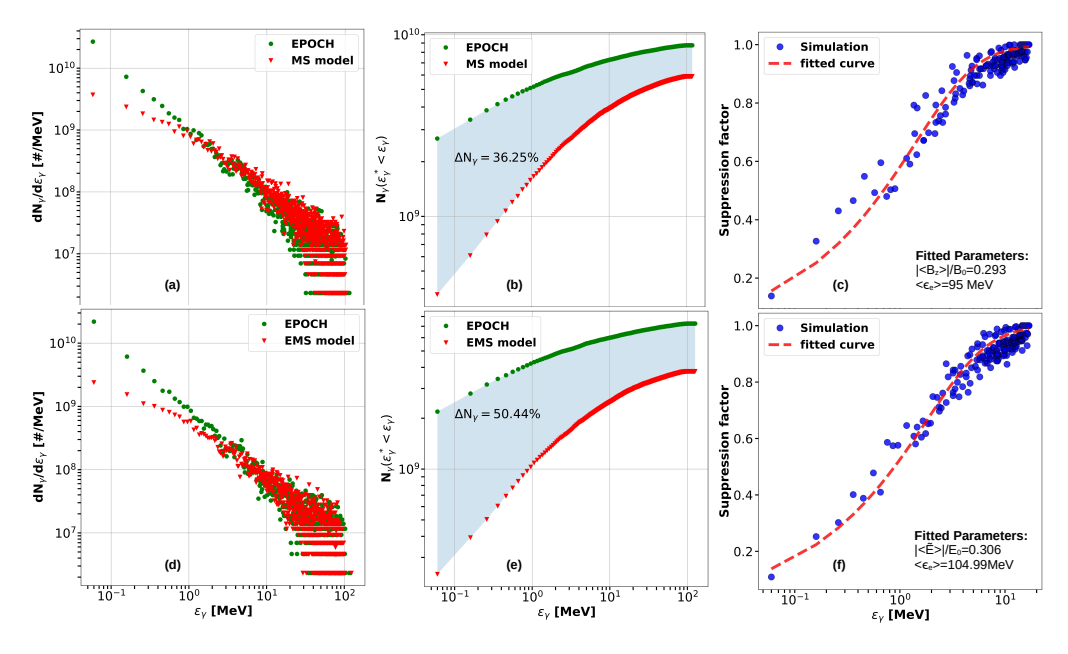


FIG. 3. Comparison of (a)&(d) the energy distribution of bremsstrahlung, (b)&(e) their corresponding accumulated number of photons with  $\epsilon_{\gamma}^* < \epsilon_{\gamma}$ , defined by Eq.20, as a function of  $\epsilon_{\gamma}$ , for the magnetic suppression (MS) as well as the electric and magnetic suppression (EMS) models. The analysis was conducted for a subset of radiating electrons with an average energy of between 95 MeV and 105 MeV that passed through regions with normalized fields of 0.29 - 0.31. Panels (c)&(f) show curve-fitting (red dashed-curve) of PIC simulation data for the suppression factors obtained from two suppression models (filled-blue circles).

In order to gain more insight into the suppression effect at the microscopic level, we tracked the number of energetic electrons accelerated within the channel. Their trajectories are shown in Fig. 4(a) and 4(b) (see the black and color lines). These electrons were randomly selected at t = 185 fs from the electrons with energy above 500 MeV. We provide simulations with and without electric-magnetic field suppression effects. For both of them, we find that the electrons are injected from the periphery of the channel near the entrance and accelerated by the intense laser pulse in the forward direction. We observe, similar to Gong<sup>17</sup>, that these trajectories are confined within a magnetic boundary  $R_{\rm MB} (\approx 1 \ \mu {\rm m})$  that is smaller than the initial channel radius  $R_{\rm ch}=1.8~\mu{\rm m}$ . The locations of the emission events along each trajectory are indicated by the black circles. Qualitatively, both panels show similar trajectories, but fewer emission vertices can be identified for the simulation, including suppression. This finding is corroborated by overlaying the counts of low-energy (< 10 MeV) bremsstrahlung generated per cell and integrated until simulation time t = 185 fs as a colored background. As illustrated by the figures, the simulation employing the suppression effect Fig. 4(b) appears to result in less localization of low-energy emissions within the channel than the simulation without suppression Fig. 4(a).

These suppression levels, as seen in the previous section, are quite comparable for magnetic suppression and electric and magnetic suppression effects. In order to further investigate this observation, we traced the fields accelerating the color-highlighted electrons from Fig. 4(b) throughout their passage in the plasma. Figure 5 shows the temporal history of the normalized transverse electric  $E_{\perp}/E_0$  and magnetic  $V_{\parallel}B_z/E_0$  components of the Lorentz force for these electrons. The field strengths are a measure of the force acting on the electrons with velocity  $V_{\parallel}$  along their trajectory, thus a measure of the deflection angle  $\Theta_{EMS}$  relevant for the bremsstrahlung suppression mechanism. We can identify two types of interactions of the electron with the electric and magnetic fields in the simulation. Until the simulation time of  $t \approx 120$  fs, the electron undergoes acceleration by relatively low strength fields at the entrance of the channel, where the magnetic and electric field components are highly uncompensated. The moment the electron is injected into the channel (after  $t \approx 120$  fs), it will be accelerated by the laser electric and magnetic fields. The transverse Lorenz force component by a plane wave exhibits high compensation between the electric and magnetic field components. This is visible in Fig. 5 for all shown electron trajectories.

Due to the above-mentioned compensation, the averaged

field strength evaluated by the electric and magnetic model of suppression amounts to a small fraction < 0.1 of the average field strength considered by the magnetic suppression model. Though the average field strengths are an order of magnitude different, the yield of bremsstrahlung photons is similar for the two models. The explanation of this behavior can be found in the slow scaling of the suppression factor, as shown by Fig. 1. For the electron energy and field strength ranges accessible by the relativistically induced transparency regime, only a few percent level differences are expected, leading in total to similar bremsstrahlung yields.

In the final part of our investigation, we studied the influence of electric and magnetic suppression on the electron

fluence of electric and magnetic suppression on the electron dynamics within the channel. Fig. 4(c) and (d) show snapshots of the momentum distribution  $(p_x, p_y)$  of all electrons in the channel at time t = 185 fs as a color map. While we can observe subtle differences in the shape of the trajectories between the two simulations, differences can be seen in the color maps of the phase-space density distribution. As the high-energy electrons are prone to undergo the electric and magnetic suppression effect, we examine in the following if a systematic different acceleration can be found or if the above observation is a transient one, the result of slight changes in the dynamics of the acceleration. We stepped back in time and examined the phase-space distribution of the electron momenta  $(x,p_x)$  and  $(x,p_y)$  at several times (exemplary we show  $(x,p_x)$  at 160 fs [see Fig. 6]). Since the magnetic field generated by the accelerated electrons effectively prevents injections into the channel apart from its entrance<sup>40</sup>, we limit our analysis to the x segment windows located around the peak of laser intensity. We can observe differences in the electron dynamics when comparing the peak momenta between the two tests, highlighted with red arrows. Although this can be explained by the fact that the electric and magnetic suppression effect induces different recoil energies, thus altering the dephasing between electron and accelerating fields, it appears not to follow a systematic pattern. We conclude that the suppression of bremsstrahlung would not degrade or improve in general the electron acceleration, but the details of the electron acceleration dynamic will be altered. For the given density of, 20ncr the probability of Bremsstrahlung emission by an electron with 100 MeV is  $\approx 10^{-4}$  for a propagation length of 10 µm. The emissions are sparse events and will not significantly alter the overall electron distribution properties.

### V. CONCLUSION

In conclusion, we have incorporated, for the first time, the electric and magnetic suppression of the bremsstrahlung mechanisms in a particle-in-cell simulation code. This allowed us to examine the influence of the high fields on suppressing bremsstrahlung emitted from high-energy electrons in the regime of relativistically induced transparency. The results demonstrate appreciable suppression of low-energy emissions due to strong macroscopic electric and magnetic fields, and this has an impact on the details of the electron acceleration dynamic.

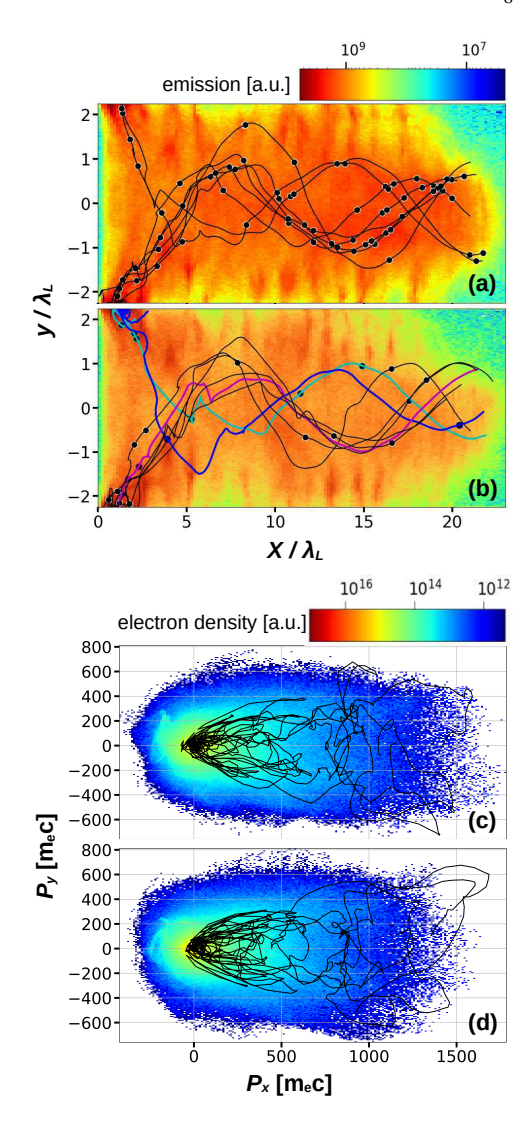
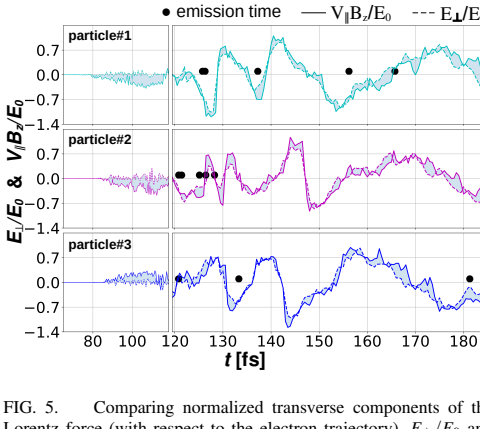


FIG. 4. Tracking trajectory of eight emitting electrons [black lines] with energy greater than 500 MeV and their location of bremsstrahlung vertices [hollow circles] inside the channel. The background color shows the snapshot of the density of emissions below 10 MeV emitted by the electrons with energy greater than 95 MeV integrated until t=185 fs for simulations from (a) EPOCH and (b) the electric and magnetic suppression model. A snapshot of the phase-space of all electrons for (c) EPOCH and (d) the electric and magnetic suppression model.

This is the author's peer reviewed, accepted manuscript. However, the online version of record will be different from this version once it has been copyedited and typeset

PLEASE CITE THIS ARTICLE AS DOI: 10.1063/5.0167288



· emission time

Comparing normalized transverse components of the Lorentz force (with respect to the electron trajectory),  $E_{\perp}/E_0$  and  $V_{\parallel}B_z/E_0$ , for the three highlighted electrons in Fig. 4(b).

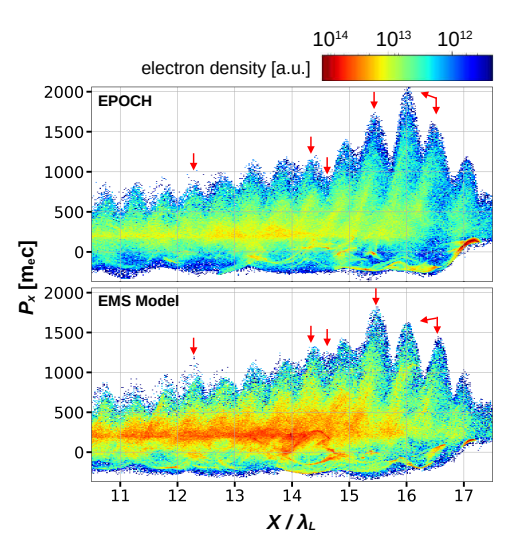


FIG. 6. Snapshots of longitudinal  $p_x$ , the phase-space density distribution of accelerated electrons with energy above 95 MeV at 160 fs from EPOCH, and the electric and magnetic suppression (EMS) model. The maximal momentum is found at different positions, a signature of a distinct acceleration history.

Furthermore, the analyses performed indicated notable disparities in the electron dynamics with and without suppression mechanism. One possible explanation for these discrepancies could be variations in recoil energies employed by the EMS effect, which could subsequently alter the dephasing between the electron and accelerating fields. However, these discrepancies did not demonstrate any systematic pattern. This leads us to conclude that while bremsstrahlung suppression does not categorically enhance or degrade electron acceleration, it unquestionably influences the specific characteristics of electron acceleration dynamics.

### **ACKNOWLEDGMENTS**

This research was supported by AFOSR (Grant No. FA9550-17-1-0382) and by the National Science Foundation - Czech Science Foundation partnership (NSF award PHY-2206777). Simulations were performed with EPOCH (developed under UK EPSRC Grants EP/G054950/1, EP/G056803/1, EP/G055165/1 and EP/ M022463/1).

- <sup>1</sup>J. Daugherty and R. W. Bussard, "Pair annihilation in superstrong magnetic fields," Astrophysical Journal, Part 1, vol. 238, May 15, 1980, p. 296-310. 238, 296-310 (1980).
- <sup>2</sup>A. K. Harding, "Physics in strong magnetic fields near neutron stars," Science **251**, 1033–1038 (1991).
- <sup>3</sup>M. A. Liberman and B. Johansson, "Properties of matter in ultrahigh magnetic fields and the structure of the surface of neutron stars," Physics-Uspekhi 38, 117 (1995).
- <sup>4</sup>M. G. Baring and A. K. Harding, "Radio-quiet pulsars with ultrastrong magnetic fields," The Astrophysical Journal 507, L55 (1998).
- <sup>5</sup>D. Wickramasinghe and L. Ferrario, "Magnetism in isolated and binary white dwarfs," Publications of the Astronomical Society of the Pacific 112,
- <sup>6</sup>R. Turolla, S. Zane, and A. Watts, "Magnetars: the physics behind observations. a review," Reports on Progress in Physics 78, 116901 (2015).
- <sup>7</sup>C. N. Danson, C. Haefner, J. Bromage, T. Butcher, J.-C. F. Chanteloup, E. A. Chowdhury, A. Galvanauskas, L. A. Gizzi, J. Hein, D. I. Hillier, et al., "Petawatt and exawatt class lasers worldwide," High Power Laser Science and Engineering 7, e54 (2019).
- <sup>8</sup>J. W. Yoon, C. Jeon, J. Shin, S. K. Lee, H. W. Lee, I. W. Choi, H. T. Kim, J. H. Sung,  $\,$  and C. H. Nam, "Achieving the laser intensity of 5.5  $\!\times$   $\,10$ 22 w/cm 2 with a wavefront-corrected multi-pw laser," Optics express 27, 20412-20420 (2019).
- <sup>9</sup>F. Lureau, G. Matras, O. Chalus, C. Derycke, T. Morbieu, C. Radier, O. Casagrande, S. Laux, S. Ricaud, G. Rey, et al., "High-energy hybrid femtosecond laser system demonstrating  $2\times 10$  pw capability," High Power Laser Science and Engineering 8, e43 (2020).
- <sup>10</sup>C. Radier, O. Chalus, M. Charbonneau, S. Thambirajah, G. Deschamps, S. David, J. Barbe, E. Etter, G. Matras, S. Ricaud, et al., "10 pw peak power femtosecond laser pulses at eli-np," High Power Laser Science and Engineering 10, e21 (2022).
- 11 See, https://eli-laser.eu/.
- <sup>12</sup>See, http://www.xcels.iapras.ru/
- <sup>13</sup>B. F. Lasinski, A. B. Langdon, S. P. Hatchett, M. H. Key, and M. Tabak, "Particle-in-cell simulations of ultra intense laser pulses propagating through overdense plasma for fast-ignitor and radiography applications, Physics of Plasmas 6, 2041-2047 (1999).
- <sup>14</sup>S. Bulanov, D. Dylov, T. Z. Esirkepov, F. Kamenets, and D. Sokolov, "Ion acceleration in a dipole vortex in a laser plasma corona," Plasma physics reports 31, 369–381 (2005).

  15T. Nakamura, S. V. Bulanov, T. Z. Esirkepov, and M. Kando, "High-energy
- ions from near-critical density plasmas via magnetic vortex acceleration, Physical review letters 105, 135002 (2010).
- Talyska Isrien Betas Joy.
  Ji S. Steinke, J.-L. Vay, C. G. Geddes,
  C. B. Schroeder, W. P. Leemans, T. Schenkel, et al., "Ion acceleration in laser generated megatesla magnetic vortex," Physics of Plasmas 26 (2019).
- "TZ, Gong, F, Mackenroth, T, Wang, X, Yan, T, Toncian, A. Arefiev, et al.,
  "Direct laser acceleration of electrons assisted by strong laser-driven azimuthal plasma magnetic fields," Physical Review E 102, 013206 (2020).
- <sup>18</sup>P. Kaw and J. Dawson, "Relativistic nonlinear propagation of laser beams in cold overdense plasmas," The Physics of Fluids 13, 472–481 (1970).
- <sup>19</sup>S. Harris, "Electromagnetically induced transparency in an ideal plasma," Physical review letters 77, 5357 (1996).

# accepted manuscript. However, the online version of record will be different from this version once it has been copyedited and typeset This is the author's peer reviewed,

PLEASE CITE THIS ARTICLE AS DOI: 10.1063/5.0167288

- <sup>20</sup>F. Cattani, A. Kim, D. Anderson, and M. Lisak, "Threshold of induced transparency in the relativistic interaction of an electromagnetic wave with overdense plasmas," Physical Review E 62, 1234 (2000).
- <sup>21</sup>V. Goloviznin and T. Schep, "Self-induced transparency and self-induced opacity in laser-plasma interactions," Physics of Plasmas 7, 1564–1571 (2000).
- <sup>22</sup>M. Tushentsov, A. Kim, F. Cattani, D. Anderson, and M. Lisak, "Electromagnetic energy penetration in the self-induced transparency regime of relativistic laser-plasma interactions," Physical review letters 87, 275002 (2001).
  <sup>23</sup>V. Eremin, A. Korzhimanov, and A. Kim, "Relativistic self-induced trans-
- <sup>23</sup>V. Eremin, A. Korzhimanov, and A. Kim, "Relativistic self-induced transparency effect during ultraintense laser interaction with overdense plasmas: Why it occurs and its use for ultrashort electron bunch generation," Physics of Plasmas 17 (2010).
- <sup>24</sup>S. Palaniyappan, B. M. Hegelich, H.-C. Wu, D. Jung, D. C. Gautier, L. Yin, B. J. Albright, R. P. Johnson, T. Shimada, S. Letzring, et al., "Dynamics of relativistic transparency and optical shuttering in expanding overdense plasmas," Nature Physics 8, 763–769 (2012).
- <sup>25</sup>E. Siminos, M. Grech, S. Skupin, T. Schlegel, and V. Tikhonchuk, "Effect of electron heating on self-induced transparency in relativistic-intensity laser-plasma interactions," Physical Review E 86, 056404 (2012).
- <sup>26</sup>D. Stark, T. Toncian, and A. Arefiev, "Enhanced multi-nev photon emission by a laser-driven electron beam in a self-generated magnetic field," Physical review letters 116, 185003 (2016).
- <sup>27</sup>H. Chang, B. Qiao, T. Huang, Z. Xu, C. Zhou, Y. Gu, X. Yan, M. Zepf, and X. He, "Brilliant petawatt gamma-ray pulse generation in quantum electrodynamic laser-plasma interaction," Scientific reports 7, 45031 (2017).
- <sup>28</sup>T. Wang, X. Ribeyre, Z. Gong, O. Jansen, E. d'Humières, D. Stutman, T. Toncian, and A. Arefiev, "Power scaling for collimated γ-ray beams generated by structured laser-irradiated targets and its application to twophoton pair production," Physical Review Applied 13, 054024 (2020).
- <sup>29</sup>Y. He, T. G. Blackburn, T. Toncian, and A. V. Arefiev, "Dominance of γ-γ electron-positron pair creation in a plasma driven by high-intensity lasers," Communications Physics 4, 139 (2021).
- <sup>30</sup>Y. He, I. Yeh, T. Blackburn, and A. Arefiev, "A single-laser scheme for observation of linear breit-wheeler electron-positron pair creation," New Journal of Physics 23, 115005 (2021).
- <sup>31</sup>Y. He and A. Arefiev, "Algorithm for computing the electron-positron yield from the linear breit-wheeler process in high-intensity laser-plasma interactions," Computer Physics Communications 286, 108657 (2023).
- <sup>32</sup> K. Sugimoto, Y. He, N. Iwata, I. Yeh, K. Tangtartharakul, A. Arefiev, and Y. Sentoku, "Positron generation and acceleration in a self-organized photon collider enabled by an ultraintense laser pulse," Physical Review Letters 131, 065102 (2023).
- S. Klein, "Suppression of bremsstrahlung and pair production due to environmental factors," Reviews of Modern Physics 71, 1501 (1999).
- <sup>34</sup>S. R. Klein, "Bremsstrahlung and pair creation: Suppression mechanisms and how they affect ehe air showers," in AIP Conference Proceedings CONF-9711122, Vol. 433 (American Institute of Physics, 1998) pp. 132– 147
- <sup>35</sup>T. Arber, K. Bennett, C. Brady, A. Lawrence-Douglas, M. Ramsay, N. J. Sircombe, P. Gillies, R. Evans, H. Schmitz, A. Bell, et al., "Contemporary particle-in-cell approach to laser-plasma modelling," Plasma Physics and Controlled Fusion 57, 113001 (2015).
- <sup>36</sup> J. Vyskočil, O. Klimo, and S. Weber, "Simulations of bremsstrahlung emission in ultra-intense laser interactions with foil targets," Plasma Physics and Controlled Fusion 60, 054013 (2018).
- <sup>37</sup>S. M. Seltzer and M. J. Berger, "Bremsstrahlung spectra from electron interactions with screened atomic nuclei and orbital electrons," Nuclear Instruments and Methods in Physics Research Section B: Beam Interactions with Materials and Atoms 12, 95–134 (1985).
- <sup>38</sup>F. Wan, C. Lv, M. Jia, H. Sang, and B. Xie, "Photon emission by bremsstrahlung and nonlinear compton scattering in the interaction of ultraintense laser with plasmas," The European Physical Journal D 71, 1–8 (2017).
- <sup>39</sup>B. Martinez, E. d'Humières, and L. Gremillet, "Synchrotron radiation from ultrahigh-intensity laser-plasma interactions and competition with bremsstrahlung in thin foil targets," Physical Review Research 2, 043341 (2020).
- <sup>40</sup>A. Arefiev, A. Robinson, and V. Khudik, "Novel aspects of direct

- laser acceleration of relativistic electrons," Journal of Plasma Physics 81, 475810404 (2015).
- <sup>41</sup>N. Kaiser, "Pair production in superstrong magnetic fields," Astrophys. J 273, L17 (1983).
- <sup>42</sup>A. K. Harding, "Physics in ultra-strong magnetic fields," Proceedings of the International Astronomical Union 16, 149–161 (2020).
- <sup>43</sup>L. Fedeli, A. Sainte-Marie, N. Zaim, M. Thévenet, J.-L. Vay, A. Myers, F. Quéré, and H. Vincenti, "Probing strong-field qed with doppler-boosted petawatt-class lasers," Physical review letters 127, 114801 (2021).
- <sup>44</sup>C. Thompson and R. C. Duncan, "Neutron star dynamos and the origins of pulsar magnetism," Astrophysical Journal, Part 1 (ISSN 0004-637X), vol. 408, no. 1, p. 194-217. 408, 194-217 (1993).
- <sup>45</sup>C. Thompson, "Electrodynamics of magnetars. iii. pair creation processes in an ultrastrong magnetic field and particle heating in a dynamic magnetosphere," The Astrophysical Journal 688, 1258 (2008).
- <sup>46</sup>P. L. Gonthier, A. K. Harding, M. G. Baring, R. M. Costello, and C. L. Mercer, "Compton scattering in ultrastrong magnetic fields: numerical and analytical behavior in the relativistic regime," The Astrophysical Journal 540, 907 (2000).
- <sup>47</sup> A. K. Harding and A. G. Muslimov, "Particle acceleration zones above pulsar polar caps: electron and positron pair formation fronts," The Astrophysical Journal **508**, 328 (1998).
- <sup>48</sup>R. Ruffini, G. Vereshchagin, and S.-S. Xue, "Electron–positron pairs in physics and astrophysics: from heavy nuclei to black holes," Physics Reports 487, 1–140 (2010).
- pnystas and enveryments 487, 1–140 (2010).
   Webber, G. Simpson, and H. Cane, "Radio emission, cosmic ray electrons, and the production of gamma-rays in the galaxy," The Astrophysical Journal 236, 448–459 (1980).
- <sup>50</sup>G. B. Rybicki and A. P. Lightman, *Radiative processes in astrophysics* (John Wiley & Sons, 1991).
- <sup>51</sup>C. L. Sarazin, "X-ray emission from clusters of galaxies," Reviews of Modern Physics 58, 1 (1986).
- <sup>52</sup>S. P. Reynolds, "Supernova remnants at high energy," Annu. Rev. Astron. Astrophys. 46, 89–126 (2008).
- <sup>53</sup>S. M. White, A. O. Benz, S. Christe, F. Farnik, M. R. Kundu, G. Mann, Z. Ning, J.-P. Raulin, A. V. Silva-Valio, P. Saint-Hilaire, et al., "The relationship between solar radio and hard x-ray emission," Space science reviews 159, 225–261 (2011).
- 54A. Y. Potekhin, J. A. Pons, and D. Page, "Neutron stars—cooling and transport," Space Science Reviews 191, 239–291 (2015).
- <sup>55</sup>C. M. Johns and R. Lin, "The derivation of parent electron spectra from bremsstrahlung hard x-ray spectra," Solar physics 137, 121–140 (1992).
  <sup>56</sup>E. Asseo and D. Khechinashvili, "The role of multipolar magnetic fields in
- <sup>56</sup>E. Asseo and D. Khechinashvili, "The role of multipolar magnetic fields in pulsar magnetospheres," Monthly Notices of the Royal Astronomical Society 334, 743–759 (2002).
- <sup>57</sup>P. Haensel, A. Y. Potekhin, and D. G. Yakovlev, *Neutron Stars 1* (Springer, 2007).
- <sup>58</sup>E. García-Berro, P. Lorén-Aguilar, G. Aznar-Siguán, S. Torres, J. Camacho, L. G. Althaus, A. H. Córsico, B. Külebi, and J. Isern, "Double degenerate mergers as progenitors of high-field magnetic white dwarfs," The Astrophysical Journal 749, 25 (2012).
- physical Journal 747, 22 (2012).
  59A. Kostenko and C. Thompson, "Qed phenomena in an ultrastrong magnetic field. i. electron-photon scattering, pair creation, and annihilation,"
  The Astrophysical Journal 869, 44 (2018).
- <sup>60</sup>T. Wang, T. Toncian, M. Wei, and A. Arefiev, "Structured targets for detection of megatesla-level magnetic fields through faraday rotation of xfel beams," Physics of plasmas 26 (2019).
- <sup>61</sup>S. P. Hatchett, C. G. Brown, T. E. Cowan, E. A. Henry, J. S. Johnson, M. H. Key, J. A. Koch, A. B. Langdon, B. F. Lasinski, R. W. Lee, et al., "Electron, photon, and ion beams from the relativistic interaction of petawatt laser pulses with solid targets," Physics of Plasmas 7, 2076–2082 (2000).
- <sup>62</sup>J. Kmetec, C. Gordon III, J. Macklin, B. Lemoff, G. Brown, and S. Harris, "Mev x-ray generation with a femtosecond laser," Physical review letters 68, 1527 (1992).
- <sup>63</sup>C. Gahn, G. Pretzler, A. Saemann, G. Tsakiris, K. Witte, D. Gassmann, T. Schätz, U. Schramm, P. Thirolf, and D. Habs, "Mev γ-ray yield from solid targets irradiated with fs-laser pulses," Applied physics letters 73, 3662–3664 (1998).
- <sup>64</sup>A. Henderson, E. Liang, N. Riley, P. Yepes, G. Dyer, K. Serratto, and P. Shagin, "Ultra-intense gamma-rays created using the texas petawatt

Physics of Plasmas

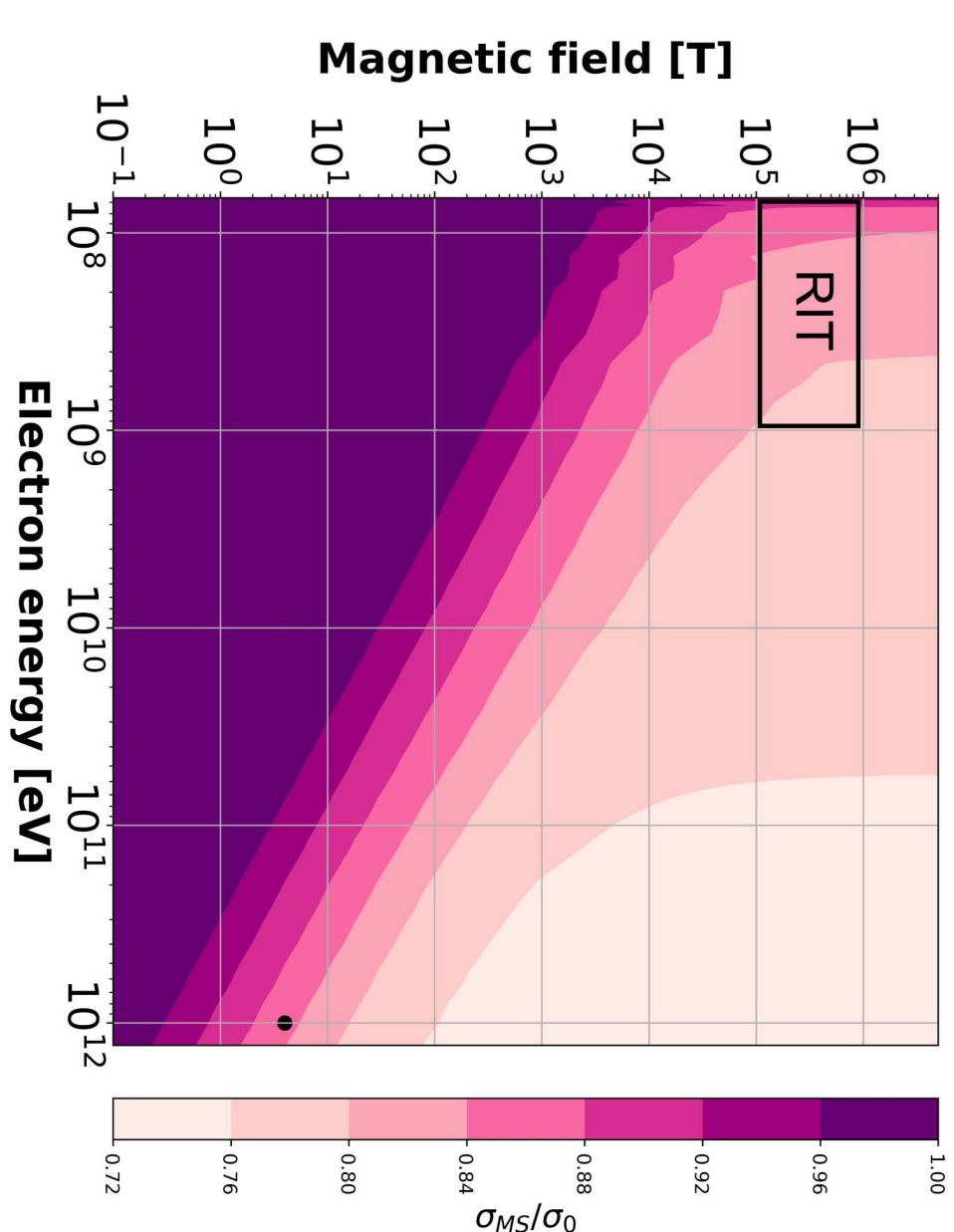
This is the author's peer reviewed, accepted manuscript. However, the online version of record will be different from this version once it has been copyedited and typeset.

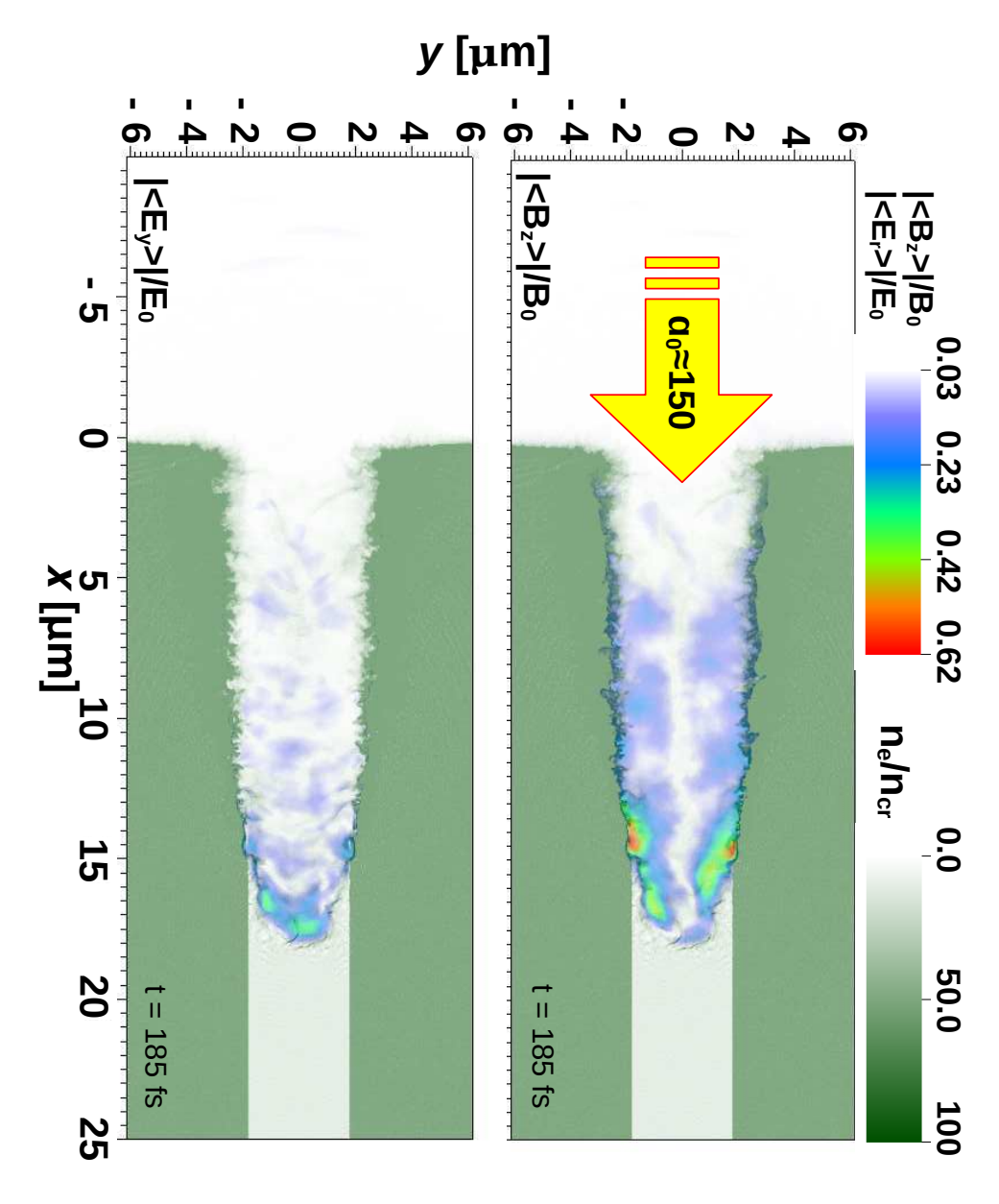
PLEASE CITE THIS ARTICLE AS DOI: 10.1063/5.0167288

- laser," High Energy Density Physics 12, 46–56 (2014).

  65 M. L. Perl, "Notes on the landau, pomeranchuk, migdal effect: Experiment
- and theory," Tech. Rep. (SCAN/9408125, 1994).

  66P. Anthony, R. Becker-Szendy, P. Bosted, M. Cavalli-Sforza, L. Keller, L. Kelley, S. Klein, G. Niemi, M. L. Perl, L. Rochester, et al., "An accurate measurement of the landau-pomeranchuk-migdal effect," Physical Review Letters 75, 1949 (1995).
- <sup>67</sup>P. Anthony, R. Becker-Szendy, P. Bosted, M. Cavalli-Sforza, L. Keller, L. Kelley, S. Klein, G. Niemi, M. L. Perl, L. Rochester, *et al.*, "Measurement of dielectric suppression of bremsstrahlung," Physical review letters 76, 3550 (1996).
- <sup>68</sup> V. N. Baier and V. M. Katkov, "Concept of formation length in radiation theory," Physics reports 409, 261-359 (2005).

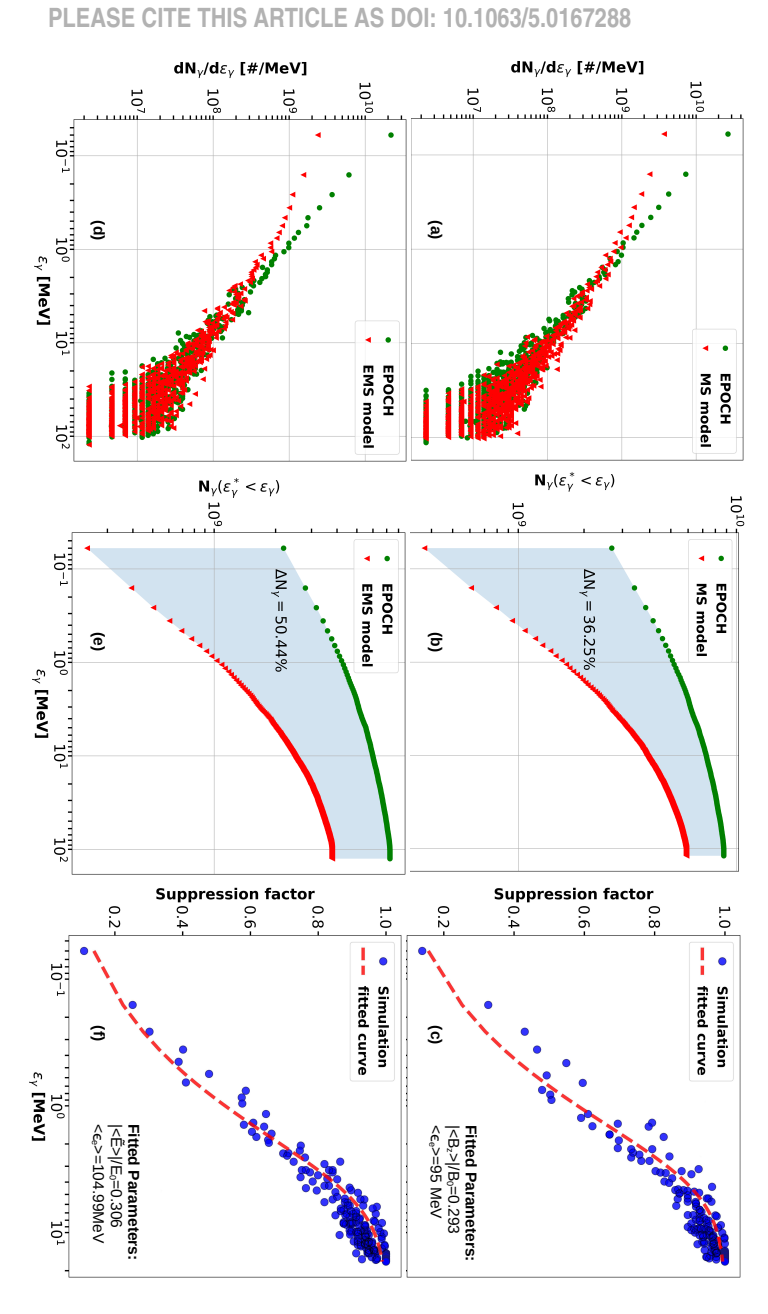




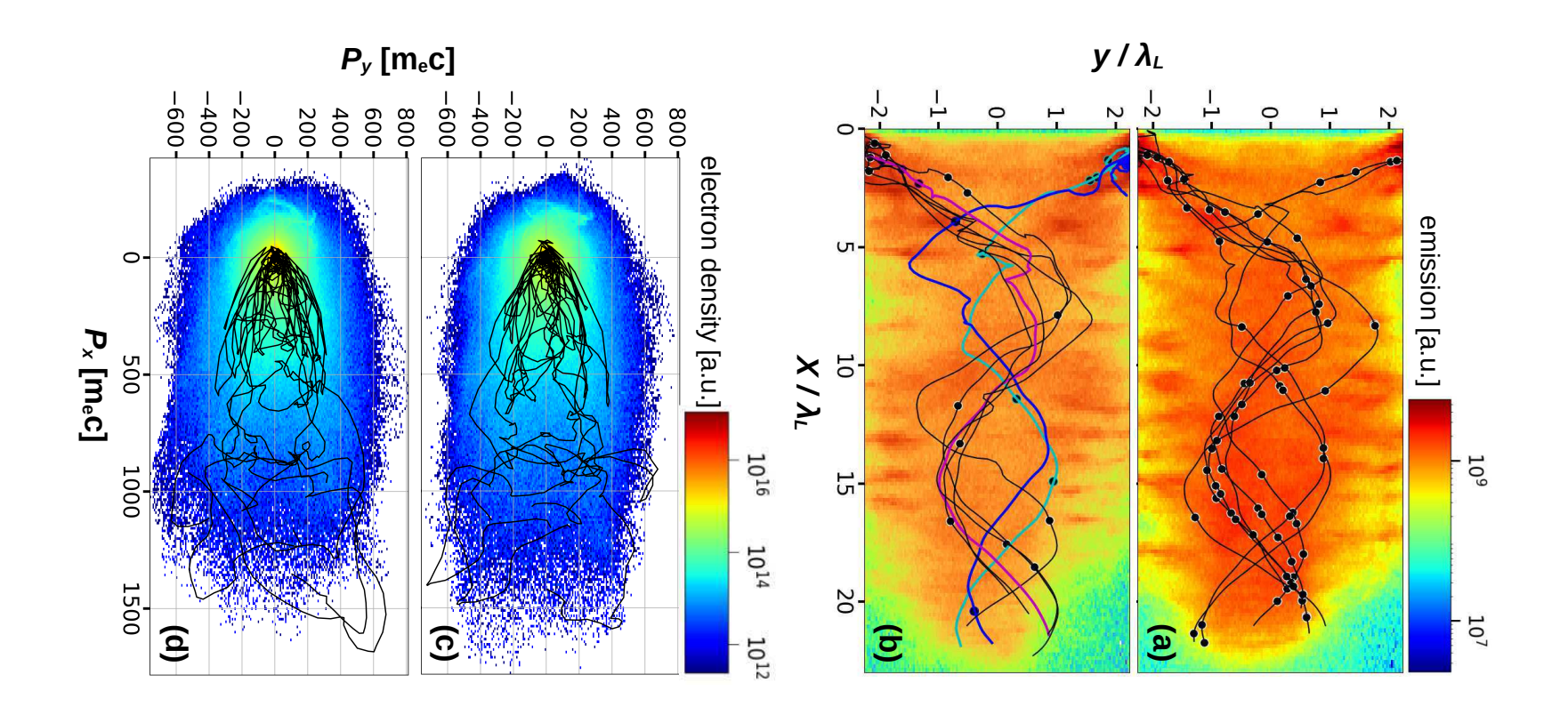
## **Physics of Plasmas**

## **ACCEPTED MANUSCRIPT**

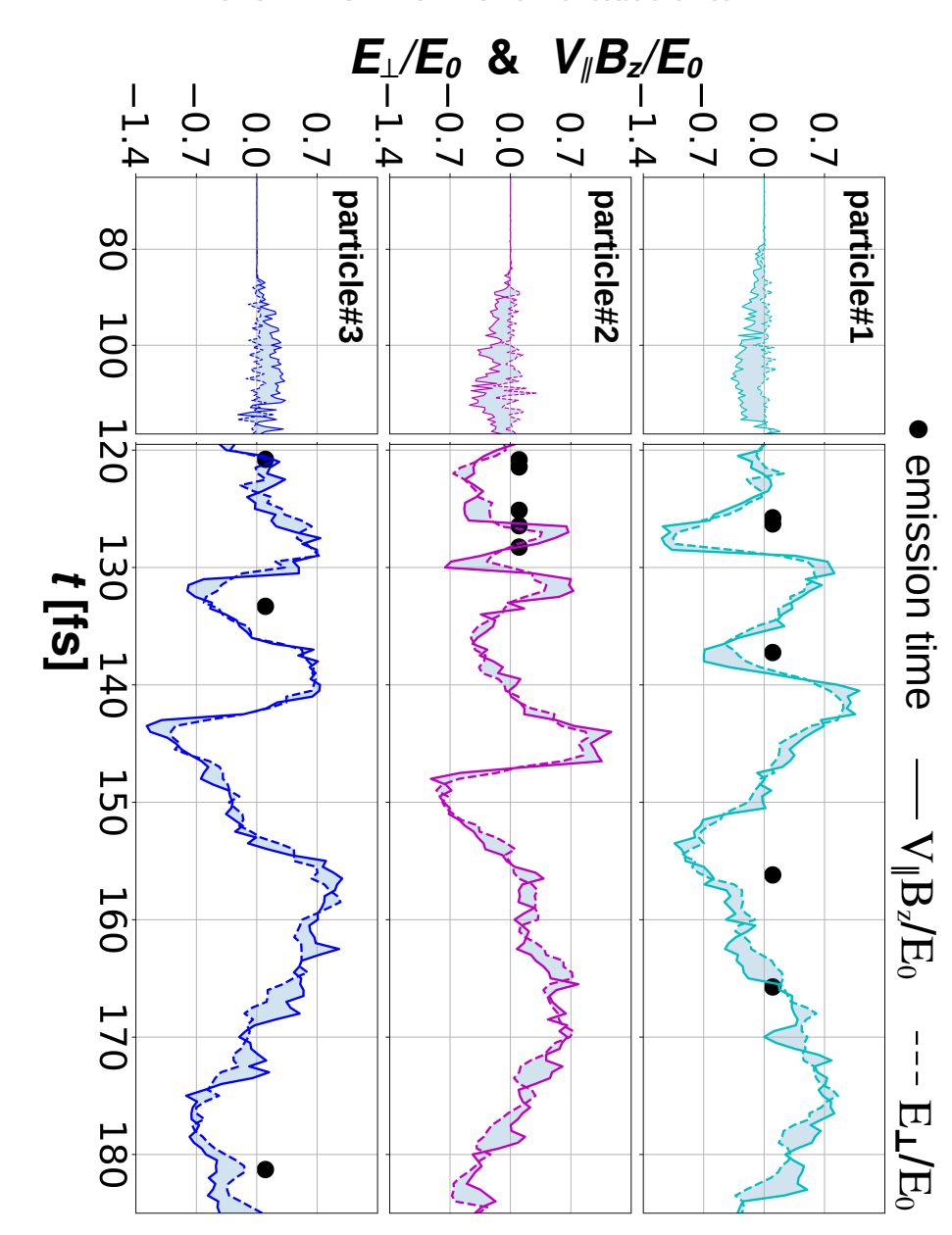
This is the author's peer reviewed, accepted manuscript. However, the online version of record will be different from this version once it has been copyedited and typeset.



# Physics of Plasmas ACCEPTED MANUSCRIPT



# Physics of Plasmas ACCEPTED MANUSCRIPT



# Physics of Plasmas ACCEPTED MANUSCRIPT

